SCIENCE CHINA
Chemistry

•ARTICLES•

March 2021 Vol.64 No.3: 419–425
https://doi.org/10.1007/s11426-020-9886-5

Arylazopyrazole-functionalized photoswitchable octanuclear Zn(II)-silsesquioxane nanocage

Kai Sheng[1], Ya-Nan Liu[2], Rakesh Kumar Gupta[2*], Mohamedally Kurmoo[4] & Di Sun[2,3*]

[1]*School of Aeronautics, Shandong Jiaotong University, Ji'nan 250037, China;*
[2]*School of Chemistry and Chemical Engineering, State Key Laboratory of Crystal Materials, Shandong University, Ji'nan 250100, China;*
[3]*Shandong Provincial Key Laboratory of Chemical Energy Storage and Novel Cell Technology, School of Chemistry and Chemical Engineering, Liaocheng University, Liaocheng 252000, China;*
[4]*Institut de Chimie de Strasbourg, Universite de Strasbourg, CNRS-UMR 7177, 4 rue Blaise Pascal, Strasbourg Cedex 67008, France*

Received September 13, 2020; accepted October 9, 2020; published online December 30, 2020

Photoswitchable organic materials have shown significant advancement for photonic applications, however, the polynuclear metal clusters conjugated with photoswitching properties are still formidable. Herein, a novel octanuclear Zn(II) nanocage {[Zn_8-($Me_4Si_4O_8$)$_2$(azopz)$_8$]•4CH_2Cl_2•MeOH•MeCN} (**SD/Zn8**) (Hazopz=3,5-dimethyl-4-(phenyldiazenyl)-1*H*-pyrazole), based on multidentate silsesquioxane and pyrazole modified by photoisomerizable azo group has been designed and synthesized to realize the reversible photoswitching behavior. X-ray crystallographic study reveals that the unique metal core consists of two annular $Me_4Si_4O_8^{4-}$ sandwiching a ring of eight Zn atoms where the pyrazole end of azopz$^-$ bridges them together. The azopz$^-$ ligands diverge above and below the plane defined by eight Zn atoms. Importantly, **SD/Zn8** shows quick *trans*-to-*cis* transformation upon 365 nm light irradiation, which can be easily changed back by 450 nm light, but slow *cis*-to-*trans* reversibility at room temperature as confirmed by UV-Vis and ^{1}H NMR spectroscopies. This process, which presumably regulates the spaces, acts like a pump and is completely repetitive. As such, it can be considered as a molecular pump energized by light. Importantly, the molecule is an energy reservoir where it absorbs the light energy and releases it slowly with time.

silsesquioxane, metal-organic nanocage, photochromism, X-ray single-crystal structure

Citation: Sheng K, Liu YN, Gupta RK, Kurmoo M, Sun D. Arylazopyrazole-functionalized photoswitchable octanuclear Zn(II)-silsesquioxane nanocage. *Sci China Chem*, 2021, 64: 419–425, https://doi.org/10.1007/s11426-020-9886-5

1 Introduction

For their potential applications such as optoelectronic devices and data storage, photoswitchable molecules are becoming an essential part of functional material chemistry [1−7]. There is a subject of current research interest in the design and synthesis of photoswitchable materials combining other intrinsic properties from the metal centers, for example, magnetism, catalysis, or biological properties [8−10]. When the materials with pores allowing the possibility of exchange, modulation of the properties mentioned above, they can be used as optical sensors through their dependence on external chemical and physical stimuli [11,12].

Reversible photoswitching of azobenzene derivatives and their metal complexes have been well explored, but the metal clusters covered by analogous heteroarene azo ligand have been rarely investigated [13−20]. Recent studies revealed that some novel arylazopyrazole-based molecular photoswitches exhibit improved reversible photoisomerization among the *trans* and *cis* isomers than azobenzene derivatives [21−24]. The *cis* and *trans* isomers of arylazopyrazole derivatives have distinct π-π* and n-π* transitions that can be distinguishable by the naked eye and interconverted by UV

*Corresponding authors (email: rkg@sdu.edu.cn; dsun@sdu.edu.cn)

(*trans*-to-*cis*) and visible light (*cis*-to-*trans*). The most thermodynamically stable isomer is the *trans*-isomer, and its photogenerated *cis*-isomer has excellent long-term thermal stability extending to ~1,000 days [21]. On the other hand, functionalized pyrazoles are extensively used as ligands to construct a diverse range of metal complexes and infinite networks [25−27]. They became very popular in the study of spin-crossover iron compounds for their moderate crystal fields [28,29]. Therefore, for the present work we selected an arylazo derivative functionalized with pyrazole as a bidentate coordination site on one side and a non-coordinating phenyl group at the other as a ligand to construct a photoswitchable zinc nanocage.

Metal-organic nanocages (MONCs) have intrigued great interest due to their unique structures and myriad applications in catalysis, sensing, and molecular magnetism [30−32]. The rational design and selection of ligands with multiple coordination sites are prerequisite to construct MONCs [33−35]. In particular, silsesquioxane $(RSiO_{1.5})_n$ ligands with multiple terminal O sites have a strong tendency to ligate with a wide range of metal ions to construct MONCs [36−38]. The precursor $\{RSi(OR')_3\}$ can be converted into cyclic, noncyclic, polycyclic matrixes, or oligomeric species depending on the hydrolysis, condensation, and reaction conditions [36−38]. Indeed, a plethora of silsesquioxane-based MONCs containing Fe(III) [39,40], Co(II) [41,42], Ni(II) [43−45], Cu(II) [46−51], Cd(II) [52], and mixed-metal [53,54] have been documented. However, Zn(II)-silsesquioxane nanocages are quite rare, no matter to say those carrying unique photochromic properties [55]. Relying on the above considerations, we anticipated that the installation of multiple arylazo ligands to the polynuclear Zn silicate might access unique and excellent photoswitching properties compared to the mono or binuclear metal complexes. To the best of our knowledge, there is no example of the photoswitchable arylazopyrazole-functionalized polynuclear MONCs.

As a part of our ongoing research on the construction of high-nuclearity silsesquioxane based MONCs [56] and clusters [57], herein, we report for the first time a photoswitchable highest-nuclearity Zn_8 nanocage with almost 100% reversibility based on tetrameric silsesquioxane and pyrazole appended photoisomerizable ligands. **SD/Zn8** shows a space craft-like nanocage structure, comprising of an equatorial Zn_8 ring sandwiched by two $Me_4Si_4O_8^{4-}$, and further decorated by eight photoswitching azopz$^-$. In the 4-fold symmetric $Me_4Si_4O_8^{4-}$ all the O atoms facing one side and the methyl facing in the opposite orientation. The photoswitchable properties of **SD/Zn8** before and after photoirradiation were studied by UV-Vis and ^{1}H NMR spectroscopies. The results show that the isomerization efficiency of **SD/Zn8** is high to 99% in both the cases *trans*-to-*cis* and *cis*-to-*trans* isomers.

2 Results and discussion

2.1 Synthesis of SD/Zn8

The targeted Zn(II)-methylsilsesquioxane nanocage was synthesized using pre-fabricated sol which is a well-established technique used in the study of gels and glasses. The reaction involves the conversion of methyltrialkoxysilane $\{MeSi(OMe)_3\}$ to a mixture of oligomeric siloxanolate $[(MeSi(O)ONa)_n]$ species by *in situ* hydrolysis in the presence of NaOH. The next step includes the reactions of sodium siloxanolate $[(MeSi(O)ONa)_n]$, $Zn(NO_3)_2$•$6H_2O$ and ancillary ligand Hazopz in $MeCN/CH_2Cl_2$ (5 mL; *v*:*v*=4:1) under solvothermal condition at 100 °C (Scheme 1). Slow evaporation of the solvent at room temperature for 2−3 days allowed us to isolate the yellow crystals of **SD/Zn8** (Yield: 75% based on $Zn(NO_3)_2$•$6H_2O$). As shown in Figure S1 (Supporting Information online), the bulk sample was collected as crystals. Notably, the sol contains a range of polytetrahedra of $(MeSiO_2)_n$, and it was hoped that the Zn(II) ion would selectively choose one, and indeed this is the case. Our original idea for choosing the ancillary Hazopz ligand was to bridge the Zn atoms *via* the N–N of the pyrazolate end, while its other end prevents propagation, thus allowing it to realize characteristic photo-induced *trans*-*cis* isomerism. Therefore, our aim appears to be successful by achieving a unique cluster separated from each other. The solid-state structure was determined by single-crystal X-ray analysis, which revealed that it is an octanuclear Zn(II)-silsesquioxane nanocage. What was not expected was the formation of pores housing solvents in between the clusters within the unit cell. These solvent molecules are confirmed by TGA measurement (Figure S2). The weight loss of 14.20% (calcd 14.15%) can be ascribed to the removal of the solvent molecules in the pores before 250 °C. More interestingly, there is a clear platform from 250 to 400 °C indicating high thermal stability of the nanocage. **SD/Zn8** was further characterized by attenuated total reflectance infrared (ATR-IR) (Figure S3) and powder X-ray diffraction (PXRD) (Figure S4). The PXRD patterns of the bulk sample are consistent with the patterns simulated from the single-crystal X-ray data, indicating good phase purity.

2.2 Crystal structure of SD/Zn8

SD/Zn8 crystallizes in the tetragonal *P*4/*nnc* space group (Table S1, Supporting Information online) where the asymmetric unit contains two independent Zn atoms, 1/8 $Me_4Si_4O_8^{4-}$ and one azopz$^-$. It exhibits space craft-like nanocage structure surrounded by two $Me_4Si_4O_8^{4-}$ and eight ancillary azopz$^-$ (Figure 1). Both the ligands have an approximate C_4 symmetric arrangement. All the Zn(II) ions are co-planar (Figure 1(c)) and construct an eight-membered $\{Zn_8O_8\}$ crown ether-like structure through eight μ_2-O atoms (Figure

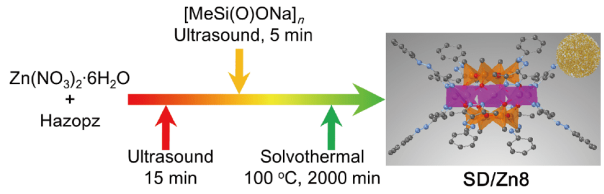

Scheme 1 Synthesis of **SD/Zn8** and its microscope appearance (color online).

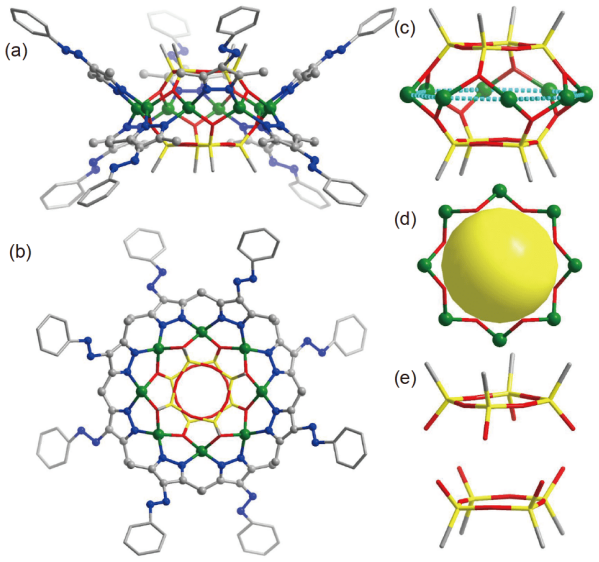

Figure 1 (a) Side and (b) top view of molecular structure of **SD/Zn8**. (c) The space craft-like skeleton of octanuclear Zn(II)-silsesquioxane nanocage. (d) The crown ether-like $\{Zn_8O_8\}$ ring. (e) The tetrameric $Me_4Si_4O_8^{4-}$ in **SD/Zn8**. Color code: Zn, green; Si, yellow; O, red; C, grey; N, blue (color online).

1(d)). All the Zn centers exhibit tetrahedral coordination geometry finished by two O atoms from two $Me_4Si_4O_8^{4-}$ and two N atoms from two azopz$^-$. Both $Me_4Si_4O_8^{4-}$ ligands adopt the same coordination mode (μ_8) to bind the Zn_8 ring using four terminal O atoms for each (Figure 1(c, e)). The Si−O bond lengths vary in the range of 1.595(4)−1.609(4) Å, and the Si−O−Si bond angle is 161.4(3)°. The two $Me_4Si_4O_8^{4-}$ are staggered at an angle of 44° (Figure S5). All the azopz$^-$ with a μ_2-κ_N^1:κ_N^1 mode are uniformly coordinated to the Zn atoms, and regularly arranged above and below closing all possible windows of the Zn_8 cage. The Zn−O, Zn−N bond lengths, and O−Zn−O, N−Zn−N, O−Zn−N angles (Table S2) are in line with the previously reported metal-silsesquioxanes [58−61]. The Zn−Zn separations are identical to 3.1301(7) Å. It should be noted that the planar ring of eight Zn tetrahedra and the cyclic tetrameric silsesquioxane is quite rare in the field of Zn-metallasiloxanes. The pyrazole and phenyl group of azobenzene deviates from the plane with an angle of 12.6°.

There are several chemical and structural characteristics of this molecule that are worth highlighting. From a synthetic point of view, the pre-fabricated sol must contain silsesquioxanes of multiple nuclearities and possibly also of different conformations. Here, only one is selectively involved in producing **SD/Zn8**, which we can assume is the most thermodynamically stable. From a structural point of view, the four directional oxygen atoms of $Me_4Si_4O_8^{4-}$ impose the C_4 symmetry of the molecule within the high symmetry *P*4/*nnc* space-group. Due to tetrahedral coordination of the Zn center, the two $Me_4Si_4O_8^{4-}$ moieties are staggered, thus allowing the favorable space for the pyrazole to bridge neighboring Zn atoms. For normal configuration, the organic ligands protrude out, four on each side of the central Zn_8 ring. It appears that the perfect looking structure satisfying bond distances and angles as well as the tetrahedral geometries of the Si and Zn centers may be accidental, but all molecular building units fit in harmony.

Furthermore, the directions of the azopz$^-$ units result in a two-sided challis so that the steric hindrance of the organic arms does not allow for a highly compact packing of the molecule (Figure 2(a)). The last point is the $Zn_8Si_8O_8$ core forms a symmetric ball with an empty cage without any accessible window, where the crystallography indicates it is empty (Figure 2(b)). Such void in crystals is naturally unexpected. Between the molecules and surrounded by the arms of the organic ligands exists a six-pole cube which possibly contains solvents, not visible crystallographically due to the disorder. Again, there is no window to access this space.

2.3 ESI-MS of SD/Zn8

The electrospray ionization mass spectrometry (ESI-MS) shown in Figure 3 features two distinct isotope-distribution envelopes (**1a** and **1b**) and two weaker ones (labeled as **1c** and **1d**) with the charge state of +1. Their formulae were assigned and listed in Table S3. The most dominant envelope **1a** centered at *m*/*z*=2719.11 is attributed to the monoprotonated parent ion of **SD/Zn8** ($[Zn_8(Me_4Si_4O_8)_2(azopz)_8\text{-}H]^+$; calcd. *m*/*z*= 2719.14), while **1b** centered at *m*/*z*=2579.03 is assigned to $[NaZn_8(Me_4Si_4O_8)_2(azopz)_6(OH)_2(H_2O)(C_2H_6O)_4]^+$ (Calcd. *m*/*z*=2579.11) which is equal to **SD/Zn8** losing two azopz$^-$ anions but adding some guest solvent molecules

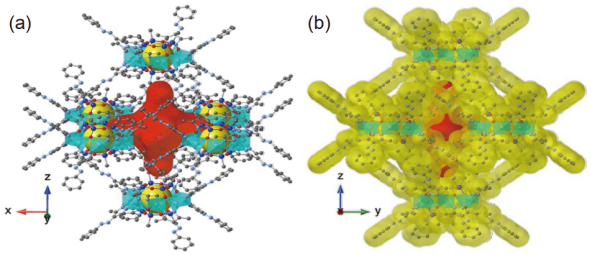

Figure 2 (a) Six neighboring Zn_8 nanocages with the internal cavity (yellow ball) around one void (red rounded octahedron). (b) The space-filling (yellow) showing no accessible window (color online).

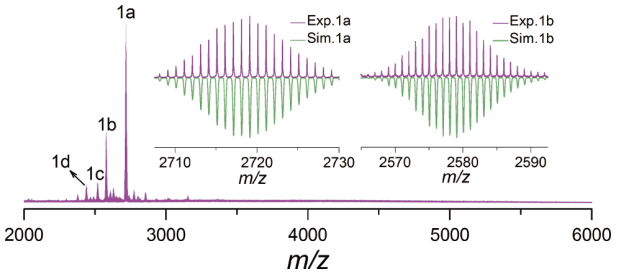

Figure 3 Positive-mode ESI-MS of **SD/Zn8** dissolved in MeOH:CH_2Cl_2 (1:1). Insets: selected experimental (purple line) and simulated (green line) isotopic envelopes (color online).

and sodium ion. The results demonstrate that **SD/Zn8** is very stable in solution although coordination-dissociation equilibrium yet exists between the ligands and solvent molecules. In order to further understand the stability and the possible fragmentation pathway of **SD/Zn8**, collision-induced dissociation (CID) mass spectrometry was performed on the parent ion **1a** at various collision energies (CEs) (Figure S6). As we can clearly see, the peak **1a** can be stable up to 40 eV. With the continuous increase of the CE to 50 eV, **1a** begins to dissociate along with the appearance of a new peak which was identified to be **1c** by careful matching the experimental and simulated isotope patterns. From 50 to 130 eV, **1a** gradually decreased while **1c** increased. At 140 eV, **1a** completely disappeared. The CID measurement also confirms the high stability of **SD/Zn8** in gas phase. At higher CE (≥50 eV), both the ligand loss and ligand exchange are involved in the fragmentation channel.

2.4 Photoisomerization studies of SD/Zn8

The photoisomerization and reversibility experiments of **SD/Zn8** were examined by UV-Vis spectroscopy. The UV-Vis absorption spectrum of the as-synthesized **SD/Zn8** in toluene (c, 2.3×10^{-5} M) shows drastic changes as a function of time using 365 nm irradiation (Figure 4(a)). At t=0, the *trans* isomer exhibits an intense absorption band at 336 nm assigned to the π-π* transition, and a weak band at 425 nm corresponding to the spin forbidden n-π* transition (Figure 4 (a), black line) [17,21,24]. As expected, increasing the irradiation time results in a hypsochromic shift of the characteristic π-π* absorption band from 336 to 294 nm accompanied by a decrease in intensity. In contrast, the band at 425 nm exhibits a slight bathochromic shift to 439 nm with an increase in intensity. The photostationary state (PSS) at 336 nm (PSS_{336}) is attained within 10 min. Moreover, the sample exposed for a further 20 min does not show any significant spectral change (Figure S7). At the PSS the *trans*-to-*cis* ratio was found to be 20%:80%, as calculated from the UV-Vis spectra as described in the literature [62−64]. The calculation assumes that before irradiation, the absorption at 336 nm is 100% from the *trans* isomer.

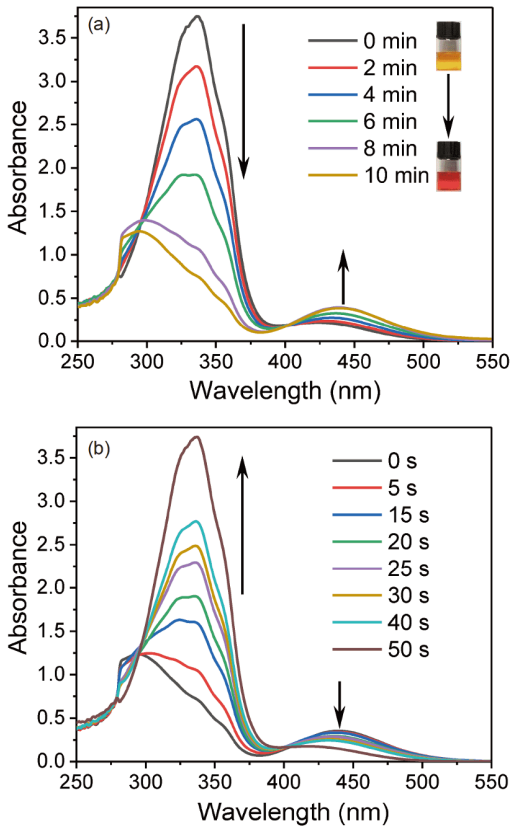

Figure 4 Temporal evolution of the UV-Vis absorption spectrum of **SD/Zn8** in toluene (c, 2.3×10^{-5} M) during irradiation with (a) 365 nm and (b) 450 nm light as a function of time (color online).

The reversible *cis*-to-*trans* photoisomerization of **SD/Zn8** was studied by irradiating with 450 nm light for different time intervals. Following the complete conversion of the *trans*-isomer to the *cis*-isomer by irradiation with 365 nm for 10 min, the temporal reversibility is recorded by irradiating with 450 nm (Figure 4(b)). The results of the *cis*-to-*trans* photoisomerization are analogous to those reported for other arylazopyrazole [21,24]. The reproducibility was studied by recording the UV-Vis spectra through alternate irradiating with 365 nm for 10 min and 450 nm for 2 min. The results for 10 cycles show complete reversibility without photodegradation, indicating its high stability under UV and visible light irradiation (Figure S8). Interestingly, **SD/Zn8** also shows reversible photoisomerization in the solid-state (Figure S9).

The long-term thermal stability of the *cis*-isomer is crucial for its applications as energy storage. Therefore, the temporal reversible *cis*-to-*trans* isomerization was measured by UV-Vis spectroscopy at room temperature. First, the **SD/Zn8** solution was exposed to 365 nm light for 10 min and stored in the dark for 12 h, then we analyzed the reverse *cis*-to-*trans* isomerization as a function of time until the original spectrum is completely recovered (Figure 5(a)). The evolution of the absorbance at 336 nm was used to calculate the first-

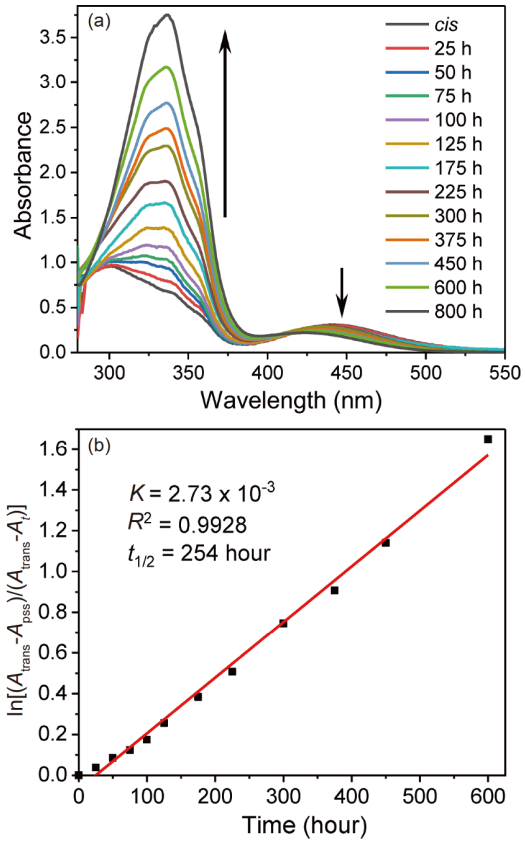

Figure 5 (a) Temporal dark *cis*-to-*trans* isomerization of **SD/Zn8** in toluene (*c*, 2.3×10^{-5} M) irradiated by 365 nm light for 10 min at room temperature, stored in the dark for 12 h; and then as a function of time until complete recovery of the original spectrum. (b) The fitting for the rate constant and half-life (color online).

order rate constant (k) and half-life ($t_{1/2}$) using the Monkowius method (Figure 5(b)) [15]. The results show that the temporal *cis*-to-*trans* isomerization is very slow at room temperature and has a longer half-life compared to those of metal complexes containing azobenzene [15]. The long half-life ($t_{1/2}$) of ~10 days is likely due to exceptional thermal stability and long lifetime of the *cis* isomer of the arylazopyrazole ligands and the stable calix-like structure of **SD/Zn8** [21,24]. It is worth noting that this *cis*-to-*trans* isomerization process can also be triggered by heat. To verify this point, we ran the control experiment by monitoring the *cis*-to-*trans* isomerization under 50 °C (Figure S10). As we expected, the results show that heat can not only trigger this *cis*-to-*trans* isomerization but also largely accelerate this transformation process. In comparison with room-temperature *cis*-to-*trans* isomerization (Figure 5(a)), it takes only *ca.* 160 min for recovering to the original spectrum at 50 °C.

2.5 Photoisomerization studies of SD/Zn8 by ^{1}H NMR spectroscopy

The diamagnetic nature of **SD/Zn8** allows us to thoroughly examine the photoinduced *trans*-to-*cis* isomerization by ^{1}H NMR spectroscopy. ^{1}H NMR spectra of **SD/Zn8** were recorded at room temperature in C_6D_6 with 365 nm irradiation as a function of time until no additional changes were observed (Figure 6). The *trans*-isomer exhibits three signals for the aromatic protons of the phenyl moiety: one doublet at 7.99 and two triplets at 7.24 and 7.11 ppm assigned to *H*c, *H*d, and *H*e, respectively. The two methyl protons of pyrazole moiety (*H*b) appear as a singlet at 2.75 ppm, while the methyl protons of $Me_4Si_4O_8^{4-}$ (*H*a) have a singlet resonance at −0.10 ppm (Figure 6(a)). After exposure of 365 nm light, all the resonances shift upfield and enhance with longer irradiation time. The phenyl protons resonate as a triplet, a doublet, and a triplet at 6.99 (*H*d), 6.93 (*H*c), and 6.81 (*H*e) ppm which indicates the existence of *cis*-isomer. The methyl protons of the pyrazole unit (*H*b) shift upfield from 2.75 to 1.71 ppm. The sharp singlet for the methyl protons of $Me_4Si_4O_8^{4-}$ moves from −0.10 to −0.28 ppm (Figure 6(b)). These significant alterations in the spectrum are attributed to the changes in the chemical environment during the photoisomerization process. The resonance of the pyrazole methyl protons (*H*b) was integrated to calculate the proportional conversion to the *cis*-isomer. After irradiating for 15 min, the percentage of the *cis*-isomer was 99%, which is higher than the results estimated by UV-Vis spectroscopy but should be more reliable. ^{1}H NMR spectroscopy further confirmed *cis*-isomer relaxes back to the *trans*-isomer in *ca.* 35 days at room temperature in the dark.

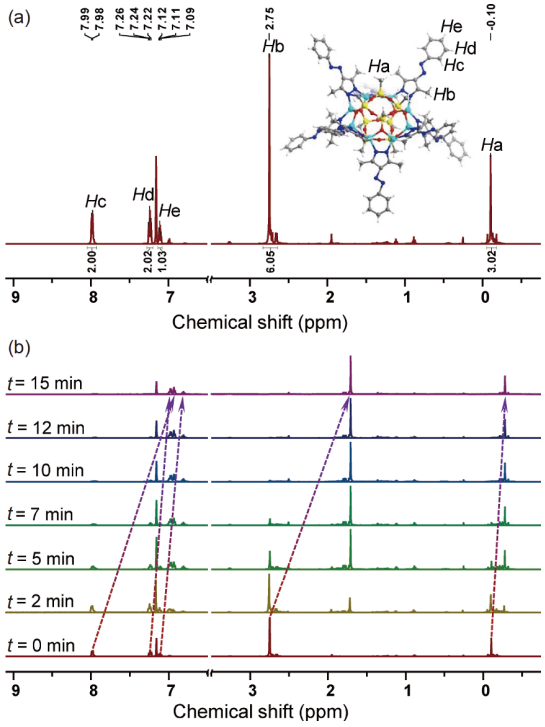

Figure 6 ^{1}H NMR spectral changes of **SD/Zn8** in C_6D_6. (a) Before irradiation (t=0, *trans*-isomer only) and (b) after irradiation with 365 nm light for t=0, 2, 5, 7, 10, 12, and 15 min, respectively (color online).

In contrast, Puddephatt *et al.* [13] have reported lower *trans*-to-*cis* conversion ratio of 75:25 for $[Pt^{II}Me_2(LL)]$ and 60:40 for $[Pt^{IV}Br_2Me_2(LL)]$, (LL=2-C_5H_4NCH=N-4-C_6H_4N =NPh) which were slightly improved in another report *viz.* 40:60 for $[PtBrMe_2(CH_2$-4-C_6H_4N=NPh)(phen)], and 25:75 for $[PtBrMe_2(CH_2$-4-C_6H_4N=NPh)(bebipy)] (phen=1,10-phenanthroline, bebipy=4,4′-bis(ethoxycarbonyl)-2,2′-bipyridine) [14]. Xie *et al*. [16] reported 56:44 conversion of a ruthenium complex containing *o*-sulfonamide azobenzene ligands. Ghebreyessus *et al*. [17] found 18:82 for $(\eta^6$-*p*-cymene)Ru(L)Cl$]^+$ (L=1-(2-methylenepyridyl)-4-(phenyldiazenyl)-3,5-dimethyl-1Hpyrazole). Han *et al*. [18] recorded 60:40 for $[PdCl_2(2Et\text{-}Azo)_2]$ (2Et-Azo=*ortho*-diethylated azobenzenes). It is worth mentioning that in the present study, **SD/Zn8** shows very rare *trans*-to-*cis* conversion ratio up to ~99% and *vice versa*, a long lifetime and high stability in contrast to other metal complexes [13–18]. These excellent photoswitching properties of **SD/Zn8** may be attributed to the highly stable nanocage structure and the installation of multiple photoisomerizable arylazopyrazole ligands possessing long-lived *cis*-isomer [21].

3 Conclusions

In summary, a novel space craft-like octanuclear Zn(II) nanocage with almost full reversible photochromism based on tetrameric silsesquioxane and pyrazole functionalized with azobenzene ligands has been developed for the first time. It consists of a ring of eight tetrahedral ZnN_2O_2 units sandwiched by the two $Me_4Si_4O_8^{4-}$ and the azopz$^-$ decorating the metal-silicate center. All the azopz$^-$ adopt the *trans*-isomer of linear configuration, and when irradiated with 365 nm light, they are progressively transformed to the *cis*-isomer with a bent configuration in less than 15 min. This process can be reversed by either irradiation with 450 nm light or heat or slowly relax in the dark over 35 days at room temperature. The ^{1}H NMR spectroscopy in solution show ~99% conversion to the *cis*-isomer. The present system is more efficient than Pt, Pd, and Ru reported in the literature. The *trans*-to-*cis* transformation is not only accompanied by color change but also the change of the void shape between the MONCs. This molecule has the potential to be a light-sensitive molecular pump. Therefore, this work can provide the basis for rational design and development of new structures showing efficient photoswitching suitable for applications using the structure-optic duality.

Acknowledgements This work was supported by the National Natural Science Foundation of China (91961105, 21822107, 21571115, 21827801), the Natural Science Foundation of Shandong Province (ZR2019ZD45, JQ201803, ZR2017MB061), the Taishan Scholar Project of Shandong Province of China (tsqn201812003, ts20190908), the Qilu Youth Scholar Funding of Shandong University, the Project for Scientific Research Innovation Team of Young Scholar in Colleges and Universities of Shandong Province (2019KJC028, 2019KJJ009) and the State Key Laboratory of Pollution Control and Resource Reuse Foundation (PCRRF18019).

Conflict of interest The authors declare no conflict of interest.

Supporting information The supporting information is available online at http://chem.scichina.com and http://link.springer.com/journal/11426. The supporting materials are published as submitted, without typesetting or editing. The responsibility for scientific accuracy and content remains entirely with the authors.

1 Gerkman MA, Sinha S, Warner JH, Han GGD. *ACS Nano*, 2019, 13: 87–96
2 Einaga Y. *J Photochem Photobiol C-Photochem Rev*, 2006, 7: 69–88
3 Natansohn A, Rochon P. *Adv Mater*, 1999, 11: 1387–1391
4 Pianowski ZL, Karcher J, Schneider K. *Chem Commun*, 2016, 52: 3143–3146
5 Bandara HMD, Burdette SC. *Chem Soc Rev*, 2012, 41: 1809–1825
6 Park J, Sun LB, Chen YP, Perry Z, Zhou HC. *Angew Chem Int Ed*, 2014, 53: 5842–5846
7 Jiang Y, Park J, Tan P, Feng L, Liu XQ, Sun LB, Zhou HC. *J Am Chem Soc*, 2019, 141: 8221–8227
8 Meng H, Zhao C, Nie M, Wang C, Wang T. *ACS Appl Mater Interfaces*, 2018, 10: 32607–32612
9 Telleria A, van Leeuwen PWNM, Freixa Z. *Dalton Trans*, 2017, 46: 3569–3578
10 Kume S, Nishihara H. *Dalton Trans*, 2008, 3260
11 Haldar R, Heinke L, Wöll C. *Adv Mater*, 2020, 32: 1905227
12 Schwartz HA, Olthof S, Schaniel D, Meerholz K, Ruschewitz U. *Inorg Chem*, 2017, 56: 13100–13110
13 Moustafa ME, McCready MS, Puddephatt RJ. *Organometallics*, 2012, 31: 6262–6269
14 Moustafa ME, McCready MS, Puddephatt RJ. *Organometallics*, 2013, 32: 2552–2557
15 Kaiser M, Leitner SP, Hirtenlehner C, List M, Gerisch A, Monkowius U. *Dalton Trans*, 2013, 42: 14749–14756
16 Deo C, Bogliotti N, Métivier R, Retailleau P, Xie J. *Organometallics*, 2015, 34: 5775–5784
17 Ghebreyessus K, Cooper Jr. SM. *Organometallics*, 2017, 36: 3360–3370
18 Han M, Hirade T, Hara M. *New J Chem*, 2010, 34: 2887–2891
19 Samanta S, Ghosh P, Goswami S. *Dalton Trans*, 2012, 41: 2213–2226
20 Moustafa ME, Boyle PD, Puddephatt RJ. *New J Chem*, 2020, 44: 2882–2889
21 Weston CE, Richardson RD, Haycock PR, White AJP, Fuchter MJ. *J Am Chem Soc*, 2014, 136: 11878–11881
22 Wang YT, Liu XY, Cui G, Fang WH, Thiel W. *Angew Chem Int Ed*, 2016, 55: 14009–14013
23 Devi S, Saraswat M, Grewal S, Venkataramani S. *J Org Chem*, 2018, 83: 4307–4322
24 Calbo J, Weston CE, White AJP, Rzepa HS, Contreras-García J, Fuchter MJ. *J Am Chem Soc*, 2017, 139: 1261–1274
25 Zhan SZ, Li M, Zhou XP, Wang JH, Yang JR, Li D. *Chem Commun*, 2011, 47: 12441–12443
26 Xiao Q, Zheng J, Li M, Zhan SZ, Wang JH, Li D. *Inorg Chem*, 2014, 53: 11604–11615
27 Dias HVR, Diyabalanage HVK, Eldabaja MG, Elbjeirami O, Rawashdeh-Omary MA, Omary MA. *J Am Chem Soc*, 2005, 127: 7489–7501
28 Halcrow MA. *Chem Soc Rev*, 2011, 40: 4119–4142
29 Halcrow MA. *Coord Chem Rev*, 2009, 253: 2493–2514
30 Ward MD, Hunter CA, Williams NH. *Acc Chem Res*, 2018, 51: 2073–2082
31 Liu ZJ, Wang XL, Qin C, Zhang ZM, Li YG, Chen WL, Wang EB.

Coord Chem Rev, 2016, 313: 94–110
32 Zhang M, Saha ML, Wang M, Zhou Z, Song B, Lu C, Yan X, Li X, Huang F, Yin S, Stang PJ. *J Am Chem Soc*, 2017, 139: 5067–5074
33 Chen W, Liao P, Yu Y, Zheng Z, Chen X, Zheng Y. *Angew Chem Int Ed*, 2016, 55: 9375–9379
34 Sun QF, Iwasa J, Ogawa D, Ishido Y, Sato S, Ozeki T, Sei Y, Yamaguchi K, Fujita M. *Science*, 2010, 328: 1144–1147
35 Fujita D, Ueda Y, Sato S, Mizuno N, Kumasaka T, Fujita M. *Nature*, 2016, 540: 563–566
36 Levitsky MM, Zubavichus YV, Korlyukov AA, Khrustalev VN, Shubina ES, Bilyachenko AN. *J Clust Sci*, 2019, 30: 1283–1316
37 Levitsky MM, Yalymov AI, Kulakova AN, Petrov AA, Bilyachenko AN. *J Mol Catal A-Chem*, 2017, 426: 297–304
38 Levitsky MM, Bilyachenko AN, Shul'pin GB. *J Organomet Chem*, 2017, 849-850: 201–218
39 Bilyachenko AN, Levitsky MM, Yalymov AI, Korlyukov AA, Vologzhanina AV, Kozlov YN, Shul'pina LS, Nesterov DS, Pombeiro AJL, Lamaty F, Bantreil X, Fetre A, Liu D, Martinez J, Long J, Larionova J, Guari Y, Trigub AL, Zubavichus YV, Golub IE, Filippov OA, Shubina ES, Shul'pin GB. *RSC Adv*, 2016, 6: 48165–48180
40 Bilyachenko AN, Levitsky MM, Yalymov AI, Korlyukov AA, Khrustalev VN, Vologzhanina AV, Shul'pina LS, Ikonnikov NS, Trigub AE, Dorovatovskii PV, Bantreil X, Lamaty F, Long J, Larionova J, Golub IE, Shubina ES, Shul'pin GB. *Angew Chem Int Ed*, 2016, 55: 15360–15363
41 Bilyachenko AN, Yalymov AI, Levitsky MM, Korlyukov AA, Es'kova MA, Long J, Larionova J, Guari Y, Shul'pina LS, Ikonnikov NS, Trigub AL, Zubavichus YV, Golub IE, Shubina ES, Shul'pin GB. *Dalton Trans*, 2016, 45: 13663–13666
42 Bilyachenko AN, Yalymov AI, Korlyukov AA, Long J, Larionova J, Guari Y, Zubavichus YV, Trigub AL, Shubina ES, Eremenko IL, Efimov NN, Levitsky MM. *Chem Eur J*, 2015, 21: 18563–18565
43 Bilyachenko AN, Yalymov A, Dronova M, Korlyukov AA, Vologzhanina AV, Es'kova MA, Long J, Larionova J, Guari Y, Dorovatovskii PV, Shubina ES, Levitsky MM. *Inorg Chem*, 2017, 56: 12751–12763
44 Bilyachenko AN, Yalymov AI, Korlyukov AA, Long J, Larionova J, Guari Y, Vologzhanina AV, Es'kova MA, Shubina ES, Levitsky MM. *Dalton Trans*, 2016, 45: 7320–7327
45 Kulakova AN, Bilyachenko AN, Korlyukov AA, Long J, Levitsky MM, Shubina ES, Guari Y, Larionova J. *Dalton Trans*, 2018, 47: 6893–6897
46 Tan G, Yang Y, Chu C, Zhu H, Roesky HW. *J Am Chem Soc*, 2010, 132: 12231–12233
47 Bilyachenko AN, Kulakova AN, Levitsky MM, Petrov AA, Korlyukov AA, Shul'pina LS, Khrustalev VN, Dorovatovskii PV, Vologzhanina AV, Tsareva US, Golub IE, Gulyaeva ES, Shubina ES, Shul'pin GB. *Inorg Chem*, 2017, 56: 4093–4103
48 Bilyachenko AN, Khrustalev VN, Zubavichus YV, Vologzhanina AV, Astakhov GS, Gutsul EI, Shubina ES, Levitsky MM. *Cryst Growth Des*, 2018, 18: 2452–2457
49 Bilyachenko AN, Levitsky MM, Khrustalev VN, Zubavichus YV, Shul'pina LS, Shubina ES, Shul'pin GB. *Organometallics*, 2018, 37: 168–171
50 Dronova MS, Bilyachenko AN, Yalymov AI, Kozlov YN, Shul'pina LS, Korlyukov AA, Arkhipov DE, Levitsky MM, Shubina ES, Shul'pin GB. *Dalton Trans*, 2014, 43: 872–882
51 Korlyukov AA, Vologzhanina AV, Buzin MI, Sergienko NV, Zavin BG, Muzafarov AM. *Cryst Growth Des*, 2016, 16: 1968–1977
52 Sergienko NV, Korlyukov AA, Arkhipov DE, Novikov VV, Eskova MA, Zavin BG. *Mendeleev Commun*, 2016, 26: 344–346
53 Gavioli G, Battistuzzi R, Santi P, Zucchi C, Pályi G, Pályi G, Ugo R, Vizi-Orosz A, Shchegolikhina OI, Pozdniakova YA, Lindeman SV, Zhdanov AA. *J Organomet Chem*, 1995, 485: 257–266
54 Astakhov GS, Bilyachenko AN, Levitsky MM, Korlyukov AA, Zubavichus YV, Dorovatovskii PV, Khrustalev VN, Vologzhanina AV, Shubina ES. *Cryst Growth Des*, 2018, 18: 5377–5384
55 Levitsky MM, Bilyachenko AN. *Coord Chem Rev*, 2016, 306: 235–269
56 Liu YN, Hou JL, Wang Z, Gupta RK, Jagličić Z, Jagodič M, Wang WG, Tung CH, Sun D. *Inorg Chem*, 2020, 59: 5683–5693
57 Liu YN, Su HF, Li YW, Liu QY, Jagličić Z, Wang WG, Tung CH, Sun D. *Inorg Chem*, 2019, 58: 4574–4582
58 Schax F, Braun B, Limberg C. *Eur J Inorg Chem*, 2014, 2014: 2124–2130
59 Pinkert D, Demeshko S, Schax F, Braun B, Meyer F, Limberg C. *Angew Chem Int Ed*, 2013, 52: 5155–5158
60 Jones MD, Keir CG, Johnson AL, Mahon MF. *Polyhedron*, 2010, 29: 312–316
61 Anantharaman G, Roesky HW, Schmidt HG, Noltemeyer M, Pinkas J. *Inorg Chem*, 2003, 42: 970–973
62 Joshi NK, Fuyuki M, Wada A. *J Phys Chem B*, 2014, 118: 1891–1899
63 Peng S, Guo Q, Hartley PG, Hughes TC. *J Mater Chem C*, 2014, 2: 8303–8312
64 Angelini G, Canilho N, Emo M, Kingsley M, Gasbarri C. *J Org Chem*, 2015, 80: 7430–7434